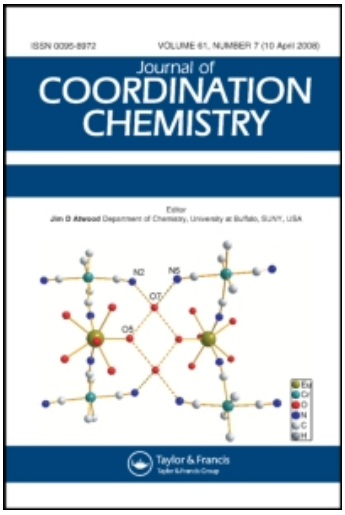

Journal of Coordination Chemistry
Publication details, including instructions for authors and subscription information:
http://www.informaworld.com/smpp/title~content=t713455674

Spectroscopic and thermal investigations of Cu(II), Zn(II), Cd(II), Pb(II) and Al(III) caproates

Moamen S. Refat[a]; Deo Nandan Kumar[b]; Robson F. De Farias[c]
[a] Faculty of Education, Department of Chemistry, Port Said, Suez Canal University, Port Said, Egypt [b] Department of Chemistry, University of Delhi, Delhi 110007, India [c] Programa de Pós-Graduação em Química, Departamento de Química, Universidade Federal do Rio Grande do Norte, 59078-970 Natal, Brazil

To cite this Article Refat, Moamen S. , Kumar, Deo Nandan and De Farias, Robson F.(2006) 'Spectroscopic and thermal investigations of Cu(II), Zn(II), Cd(II), Pb(II) and Al(III) caproates', Journal of Coordination Chemistry, 59: 16, 1857 — 1871
To link to this Article: DOI: 10.1080/00958970600662932
URL: http://dx.doi.org/10.1080/00958970600662932

Journal of Coordination Chemistry
Vol. 59, No. 16, 10 November 2006, 1857–1871

Taylor & Francis
Taylor & Francis Group

Spectroscopic and thermal investigations of Cu(II), Zn(II), Cd(II), Pb(II) and Al(III) caproates

MOAMEN S. REFAT*†, DEO NANDAN KUMAR‡ and ROBSON F. DE FARIAS§

†Faculty of Education, Department of Chemistry, Port Said, Suez Canal University, Port Said, Egypt
‡Department of Chemistry, University of Delhi, Delhi 110007, India
§Programa de Pós-Graduação em Química, Departamento de Química, Universidade Federal do Rio Grande do Norte, CP 1662, 59078-970 Natal, Rio Grande do Norte, Brazil

(*Received 20 June 2005; revised 25 September 2005; in final form 28 September 2005*)

Five complexes: $Cu(cap)_2 \cdot 4H_2O$, $Zn(cap)_2$, $Cd(cap)_2 \cdot 4H_2O$, $Pb(cap)_2$ and $Al(cap)_3 \cdot 4H_2O$ (where cap is the caproate anion $= CH_3(CH_2)_4COO^-$) were synthesized and characterized by elemental analysis, IR-spectroscopy, thermogravimetric analysis (TG), differential thermal analysis (DTA), UV-Vis spectra, ^1H NMR and X-ray powder diffraction (XRD). Using the non-isothermal, Horowitz-Metzger (HM) and Coats-Redfern methods, the kinetic parameters for the non-isothermal degradation of the complexes were calculated using TG data. The infrared and ^1H NMR data are in agreement with coordination through carboxylate, with cap acting as a bridging bidentate ligand. Thermogravimetric analysis of the hydrated complexes shows that the first degradation step is release of water molecules followed by decomposition of the anhydrous complexes, with release of caproate molecules.

Keywords: Caproic acid; Complexes; Transition and non-transition metals

1. Introduction

n-Caproic acid (*n*-hexanoic acid) (scheme 1) $C_6H_{12}O_2$, occurs in milk fats (about 2%), and in coconut oil (<1%) and is employed in the manufacture of pharmaceuticals and flavorings [1]. It is slightly soluble in water and readily soluble in ethanol and ether [2]. The binding of metal ions to carboxylic acids has been a subject of intense research with diverse applications, including as model systems for metalloactive sites in bioinorganic chemistry [3, 4]. The structural diversity encountered in metal–carboxylate complexes can be attributed to the versatile bonding of the carboxylate group which can act as a bidentate ligand or a bridging ligand [5, 6]. Compounds of transition and non-transition elements with caproic acid are not so common. A literature survey reveals that there are

*Corresponding author. Tel.: 0020127649416. Email: msrefat@yahoo.com

Journal of Coordination Chemistry
ISSN 0095-8972 print/ISSN 1029-0389 online © 2006 Taylor & Francis
DOI: 10.1080/00958970600662932

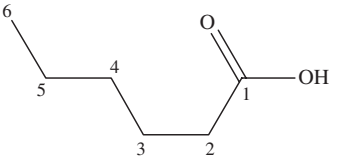

Scheme 1. Caproic acid.

some papers on the preparation of caproates of rare earth elements [7, 8] and anhydrous copper(II) hexanoate from cuprous and cupric oxides [9]. Pietsch [10] extracted caproates of thorium, lead and iron into $CHCl_3$. Caproic acid is a good extracting agent [11–13] for rare earths, zirconium, chromium, manganese, iron, gallium as well as aluminum with catechol violet by a mixture containing $CHCl_3$, caproic and propionic acids.

The present work enhances knowledge about metal-fatty acid (mono carboxylate) compounds reporting the synthesis, characterization and TG-DTA analysis of Cu(II), Zn(II), Cd(II), Pb(II) and Al(III)-caproates. By using non-isothermal TG data, kinetic parameters for thermal degradation processes were calculated through Horowitz-Metzger (HM) and Coats-Redfern (CR) methods.

2. Experimental

For all preparations, doubly distilled water was employed as solvent. All reagents were of analytical grade and were employed without further purifications. Copper(II) sulphate, Zn(II) chloride, Cd(II) nitrate, Pb(II) nitrate, and Al(III) nitrate (1 mmol, Fluka) were dissolved in 20 cm^3 of water and then the prepared solutions were slowly added to 25 cm^3 of an aqueous solution with 1 mmol of caproic acid (Fluka) under magnetic stirring. The pH of each solution was adjusted to 6–8 by addition of ammonium hydroxide. The resulting solutions were heated at 50°C and left to evaporate slowly at room temperature overnight. The obtained precipitates were filtered off, wash with hot water and dried at 60°C.

Carbon, and hydrogen elemental analysis were performed in a CHN 2400 Perkin-Elmer analyzer. The metal content was found gravimetrically by converting the compounds into their corresponding oxides. The number of crystallization water molecules was determined from TG curves. FT IR spectra were recorded on a Genesis II FT IR spectrometer in the 4000–400 cm^{-1} range with 40 scans in KBr discs. ^{1}H NMR spectra were recorded on a Bruker Advance 300 MHz equipment by using TMS as an internal standard. The electronic spectra were recorded in dimethylsulphoxide (dmso) using a Shimadzu model 1601 PC UV spectrophotometer with quartz cells of 1 cm path length. The X-ray diffraction patterns (XRD) were obtained on a Rikagu diffractometer using Cu/Kα radiation. Simultaneous TGA and DTA curves were obtained on a Rigaku 8150 thermoanalyser under static air, at a heating rate of 5 deg min^{-1}.

Table 1. Color, reaction yield and elemental analysis results for Cu(II), Zn(II), Cd(II), Pb(II) and Al(III) caproates.

			Analysis = found/(calculated) %		
Compounds	Color	Yield (%)	C	H	M
$Cu(cap)_2 \cdot 4H_2O$ Mwt = 365.55	Green	67	39.11 (39.39)	8.17 (8.21)	17.27 (17.38)
$Zn(cap)_2$ Mwt = 295.38	Silky white	65	48.53 (48.75)	7.39 (7.45)	22.08 (22.13)
$Cd(cap)_2 \cdot 4H_2O$ Mwt = 414.40	White	63	34.61 (34.75)	7.19 (7.24)	26.99 (27.12)
$Pb(cap)_2$ Mwt = 437.20	White	66	32.83 (32.94)	4.98 (5.03)	47.12 (47.39)
$Al(cap)_3 \cdot 4H_2O$ Mwt = 443.98	White	64	47.98 (48.65)	9.18 (9.23)	6.04 (6.08)

3. Results and discussion

Caproates of Zn(II), Cd(II), Pb(II), and Al(III) were obtained as white solids; Cu(II)-caproate is green. The elemental analyses summarized in table 1, as well as the TG data, are in good agreement with the proposed formulas.

3.1. *FT IR spectra*

The main ir data are summarized in table 2, and the ir spectra are shown in figure 1. The carboxylate group is able to coordinate to metal ions by three different modes, as shown in scheme 2 [14].

Type I When the carboxylate group coordinates the metal ion in a monodentate manner, the difference between the wavenumbers of the asymmetric and symmetric carboxylate stretching bands, $\Delta\nu = \nu_{as}COO^- - \nu_s COO^-$), is larger than that observed for ionic compounds.

Type II When the ligand chelates, $\Delta\nu$ is considerably smaller than that for ionic compounds, while on the asymmetric bidentate coordination, the values is in the range characteristic of monodentate coordination [15].

Type III The characteristic wavenumber difference, $\Delta\nu$, is larger than that for chelated ions and nearly the same as observed for ionic compounds.

Based on these facts it is possible to distinguish the coordination mode of the $-COO^-$ group.

Caproic acid exhibits a strong absorption band around 1700 cm^{-1} due to the C=O group. For the complexes, the differences between the asymmetrical and symmetrical vibrations (table 2b) suggest that COO^- groups are bidentate chelating (type II) [16].

3.2. *^{1}H NMR*

The ^{1}H NMR resonances are summarized in table 3, with the complexes slightly upfield compared to the free acid, indicative of the presence of free carboxylates (absence of

Table 2(a). Main infrared data for (A) $Cu(cap)_2 \cdot 4H_2O$, (B) $Zn(cap)_2$, (C) $Cd(cap)_2 \cdot 4H_2O$, (D) $Pb(cap)_2$ and (E) $Al(cap)_3 \cdot 4H_2O$ (values in cm^{-1}).

(A)	(B)	(C)	(D)	(E)	Assignments
3413s,br	–	3384s,br	–	3470 s,br	ν(OH); H_2O
3142s,br		3156s,br		3127 s,br	ν CH; CH_3
2956ms	2956s	2943s	2943mw	2941mw	ν_{as}(CH)
2927ms	2942sh 2913ms	2914s	2914mw	2913mw	
2870ms	2870w 2856w	2857s	2871ms 2857ms	2841ms	ν_s(CH)
1585vs	1528vs	1542vs	1528s	1585vs	ν_{as}(OCO)
1513ms					
1442mw	1442vs	1414vs	1457sh	1471sh	$\delta(CH_2)$
1414ms	1399vs	1328vw	1400s	1371s	ν_s(OCO)
1371s	1342s		1386sh	1314s	
1342s			1343w		
1314w					
1257mw	1285s	1271w	1286vw 1271vw	1280vw 1271vw	$\rho_w(CH_2)$
1228mw	1228s	1214w	1228s	1171ms	ν_{as}(CC)
1200s	1128ms	1171w	1128vs	1114s	
1114ms	1071ms 1014ms	1128w 1099w 1014sh	1071w 1028ms 1000w		
971vw	971ms	942w	986w	985vs	ν_s(CC)
899mw	914ms	885w	971ms 900s	942vw 871w	
857mw	842ms 743s	857w	857s 828vw	742vw	
800w			786ms		δ(CC)
728s	728ms	728ms	728w 714w	726w	δ(OCO)
671s	571ms	671w	686ms	671s	$\rho_r(H_2O)$
542w	543ms	600sh	600sh 528ms	600ms 542vw	δ(CCO) ρ_w(OCO)
457mw	457s	515ms	500ms	500ms	ν(M–O)
429mw			471sh 428s		

Table 2(b). Asymmetric and symmetric stretching vibrations of the carboxylate group, and their difference (in cm^{-1}) [$\Delta\nu = \nu_{as} - \nu_s$].

Compounds	ν_{as} (COO)	ν_s (COO)	$\Delta\nu = \nu_{as} - \nu_s$	Bonding mode
$Cu(cap)_2 \cdot 4H_2O$	1585	1371	214	Bidentate
$Zn(cap)_2$	1528	1342	186	Bidentate
$Cd(cap)_2 \cdot 4H_2O$	1542	1328	214	Bidentate
$Pb(cap)_2$	1528	1343	185	Bidentate
$Al(cap)_3 \cdot 4H_2O$	1585	1371	214	Bidentate

vs: very strong, s: strong, m: medium, w: weak, vw: very weak, br: broad. ν_{as}: asymmetric stretching; ν_s: symmetric stretching; δ: angle deformation; ρ_w: wagging mode; ρ_r: rocking mode.

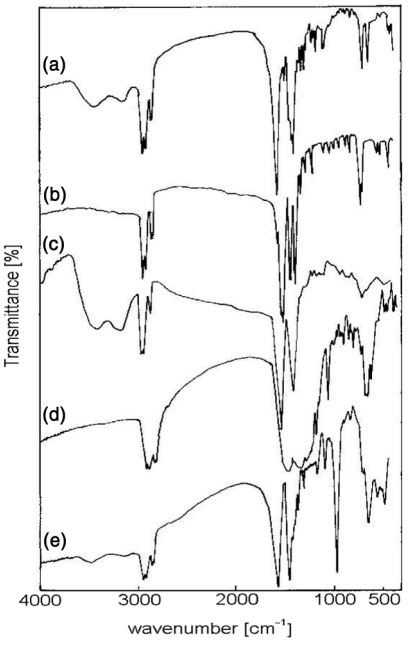

Figure 1. Infrared spectra of: (a) $Cu(cap)_2 \cdot 4H_2O$, (b) $Zn(cap)_2$, (b) $Cd(cap)_2 \cdot 4H_2O$, (d) $Pb(cap)_2$ and (e) $Al(cap)_3 \cdot 4H_2O$.

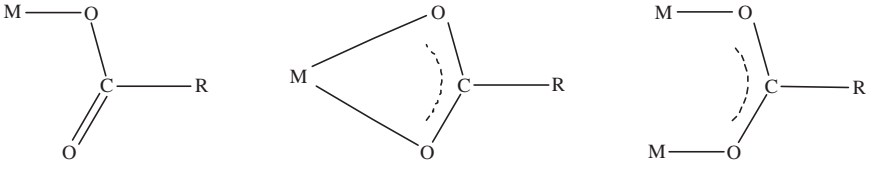

Scheme 2. Possible coordination features for the carboxylate group.

signals for COOH and OH–COOH group). A similar trend has been observed in the ^{1}H NMR spectra of metal–acid complexes [17, 18], in agreement with coordination by COO^-, as also suggested by IR data. For Cu(II), Cd(II) and Al(III) caproates, peaks in the range 2.53–2.22 ppm are from H_2O. These resonances are not present in the Zn(II) and Pb(II) caproate spectra.

3.3. *UV-Vis spectra*

The caproate compounds exhibit a strong absorption band around 260 nm and the Cu(II) caproate exhibits a peak at 660 nm. The obtained spectra are shown in figure 2. The molar absorptivities (ε_{max}) of the caproates are 9783, 10,793, 9864, 10,104 and 15,710 $mol^{-1}\,cm^{-1}$ for Cu(II), Zn(II), Cd(II), Pb(II) and Al(III), respectively. These values are almost twice the value found for caproic acid (5068), in agreement with the fact that two ligand molecules are present. In agreement with this hypothesis, the ε_{max} value for Al(III)-caproate is about three times that for free caproic acid.

Table 3. ^{1}H NMR δ values (ppm) of free caproic acid and Cu(II), Zn(II), Cd(II), Pb(II) and Al(III) caproates in dmso-d_6.

Compounds	$-CH_2$ C_2	$-CH_2$ C_3	$-CH_2$ and $-CH_2$ C_4 and C_5	$-CH_3$ C_6	Proton of H_2O	Proton of COOH
Caproic acid	2.23t	1.56m	1.29–1.33m	0.96t	–	11.00
$Cu(cap)_2 \cdot 4H_2O$	2.13t	1.55m	1.27m	0.88t	2.55	–
$Zn(cap)_2$	2.11t	1.55m	1.27m	0.87t	–	–
$Cd(cap)_2 \cdot 4H_2O$	2.16t	1.54m	1.32m	0.90t	2.57	–
$Pb(cap)_2$	2.08t	1.53m	1.30m	0.89t	–	–
$Al(cap)_3 \cdot 4H_2O$	2.18t	1.53m	1.28m	0.88t	2.53	–

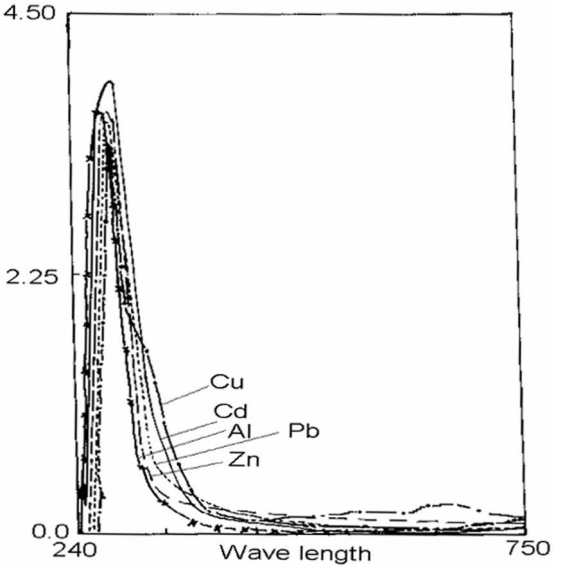

Figure 2. Electronic spectra of Cu(II), Zn(II), Cd(II), Pb(II) and Al(III)-caproate compounds.

3.4. *Thermal behavior*

The TG and DTA results are summarized in table 4 and the curves are shown in figure 3. The final products of all thermal decompositions are the oxides: MO for Cu, Zn, Cd, Pb(II) and M_2O_3 for Al(III).

The TGA and DTA curves of $Cu(cap)_2 \cdot 4H_2O$ show that this compound is thermally stable up to 353 K, when slow decomposition to CuO begins. The TG curve shows that the first mass loss between 353–538 K corresponds to the release of water, resulting in the formation of the anhydrous compound, followed by the release of the organic moiety. These assignments are confirmed by the absence of the typical OH bands on the heated samples. Furthermore, the IR spectrum of the heated sample at 538 K, after exposure to water vapor is identical to that of the starting materials. In addition, the IR spectrum of $Cu(cap)_2 \cdot 4H_2O$ recorded after heating at 673 K does not exhibit any band due to the organic moiety. Hence, the caproate of Cu(II) decomposes to oxide (CuO) with intermediate formation of basic carbonate, $CuCO_3 \cdot Cu(OH)_2$, at 661 K,

Table 4. Main TG and DTA data for the studied caproates.

Compounds	DTA results T (K) peak	TG results			
		T range (K)	Mass loss (%) Found (Calcd)	Losses	Residue
$Cu(cap)_2 \cdot 4H_2O$	374 endo	353–538	19.54 (19.69)	$4H_2O$	CuO
	545 exo	538–550	Decomposition	$2CO_2$	
	563 exo	563–870		Organic matter	
	661 exo				
$Zn(cap)_2$	410 endo	310–405	–	Moisture	ZnO
	666 exo	575–850	Decomposition	$2CO_2$	
				Organic matter	
$Cd(cap)_2 \cdot 4H_2O$	360 endo	310–407	16.34 (17.37)	$4H_2O$	CdO
	421 endo	535–730	Decomposition	$2CO_2$	
	653 exo			Organic matter	
$Pb(cap)_2$	515 exo	470–800	Decomposition	$2CO_2$	PbO
	599 endo			Organic matter	
	713 exo				
$Al(cap)_3 \cdot 4H_2O$	505 endo	490–530	17.30 (16.21)	$4H_2O$	Al_2O_3
	532 exo	530–873	Decomposition	$2CO_2$	
	657 exo			Organic matter	

(see figure 4). The most probable thermal decomposition scheme can be shown as below:

$$Cu(cap)_2 \cdot 4H_2O \xrightarrow{353-538\,K} Cu(cap)_2 \xrightarrow{673\,K} CuCO_3 \cdot Cu(OH)_2 \xrightarrow{>773\,K} CuO$$

The DTA curve for Cu(II)-caproate displays two spaced endothermic and exothermic peaks, respectively at 374 and 547 K. The inflexion points at 374 and 547 K can be attributed to the loss of water. The exothermic signal at 661 K can be attributed to decomposition of the intermediate formed, $CuCO_3Cu(OH)_2$, involving the loss of CO_2 and hydroxyl group with simultaneous formation of CuO.

The other two hydrated compounds, Cd(II) and Al(III) caproates, are stable up to 325 K and then lose four water molecules in one step (figure 3) over 407–530 K. The dehydration process is connected with an endothermic peak at 360 and 421 K for $Cd(cap)_2 \cdot 4H_2O$ and at 505 K for $Al(cap)_3 \cdot 4H_2O$. After dehydration, the anhydrous compounds decompose in different ways, stable up to 407–530 K before decomposing to oxides over 655 K. Caproates of Cd(II) and Al(III) decompose to oxides but the Cd(II) caproate compound has intermediate formation of, $CdCO_3$, at 653 K. The anhydrous Al(III) compound is not stable and decomposes directly to Al_2O_3. These steps are supported by the IR spectra obtained for the products in different decomposition steps, as shown in figure 4. The proposed thermal degradation sequences are:

$$Cd(cap)_2 \cdot 4H_2O \rightarrow Cd(cap)_2 \rightarrow CdCO_3 \rightarrow CdO$$

$$Al(cap)_3 \cdot 4H_2O \rightarrow Al(cap)_3 \rightarrow Al_2O_3$$

The decomposition proceeds via one and three steps for Zn(II) and Pb(II) caproates, respectively. In the DTA curves, there are exothermic peaks at 666 K for Zn(II)

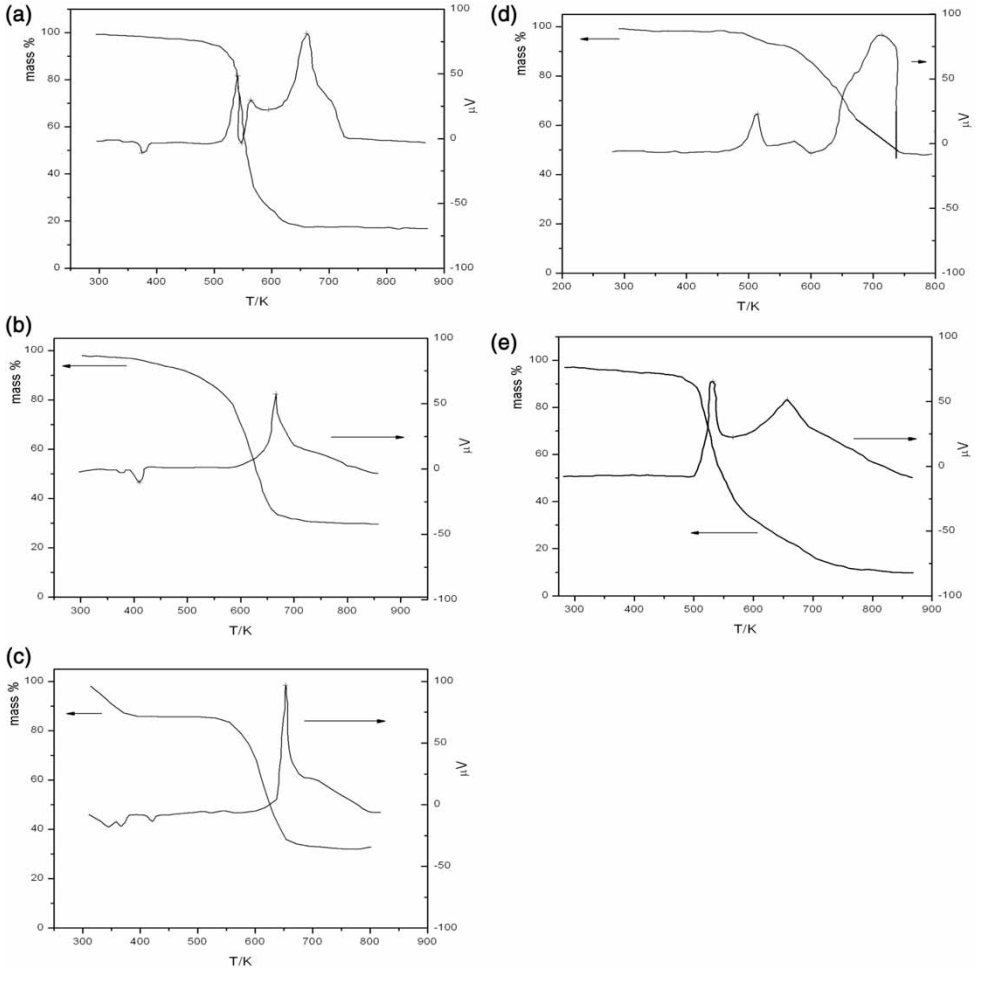

Figure 3. TGA and DTA curves of: (a) $Cu(cap)_2 \cdot 4H_2O$, (b) $Zn(cap)_2$, (b) $Cd(cap)_2 \cdot 4H_2O$, (d) $Pb(cap)_2$ and (e) $Al(cap)_3 \cdot 4H_2O$.

and at 515, 599 and 713 K for Pb(II). The most probable thermal decomposition sequences are:

$$Zn(cap)_2 \rightarrow ZnO$$

$$Pb(cap)_2 \rightarrow PbCO_3 \rightarrow PbO$$

The proposed decomposition sequence implies that the zinc caproate decomposes directly to zinc oxide, in agreement with the presence of a single peak in the DTA curve. On the other hand, the lead(II) caproate, exhibits three peaks at 515, 599 and 713 K. The first two are associated with the formation of $PbCO_3$ (which is detected in IR spectra of thermal decomposition product) and the last one with the formation of yellow PbO.

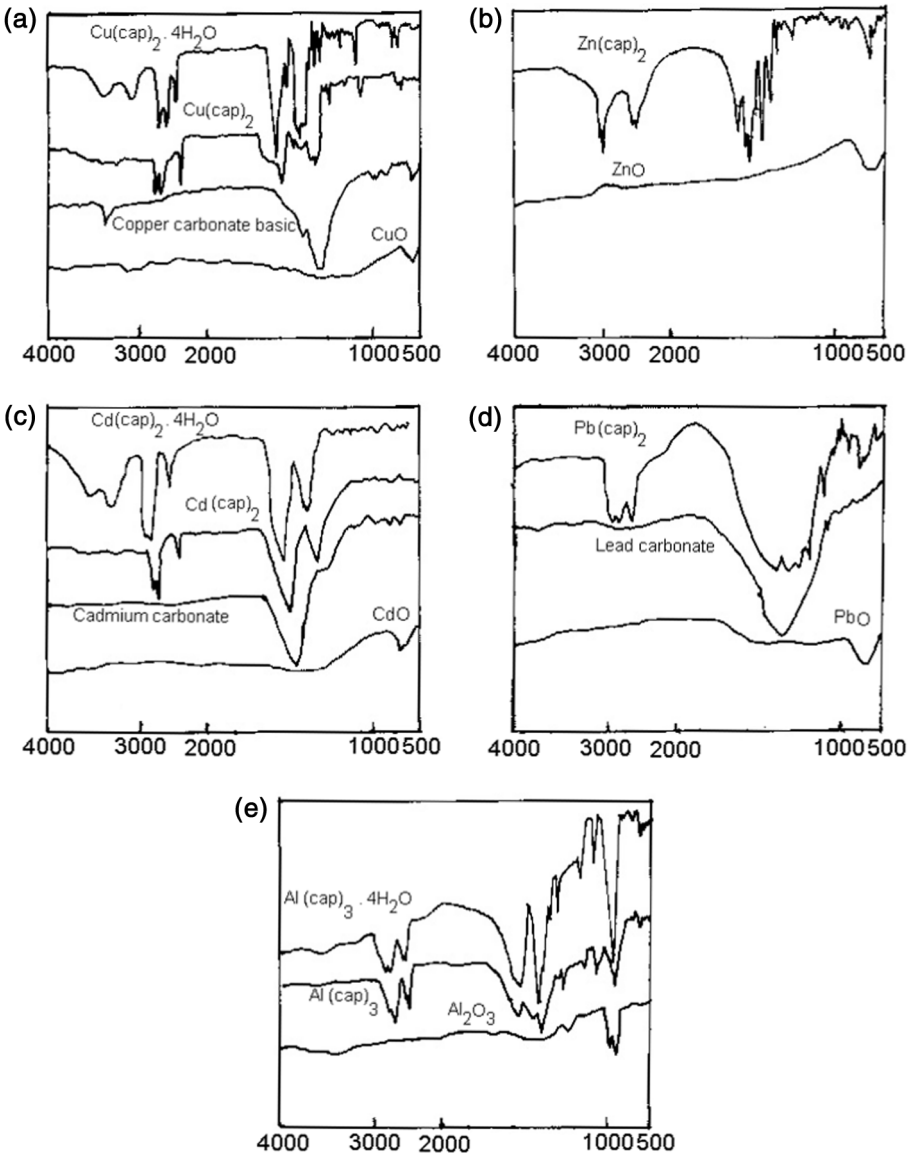

Figure 4. Infrared spectra of the degradation steps of: (a) $Cu(cap)_2 \cdot 4H_2O$, (b) $Zn(cap)_2$, (c) $Cd(cap)_2 \cdot 4H_2O$, (d) $Pb(cap)_2$ and (e) $Al(cap)_3 \cdot 4H_2O$.

3.5. *Kinetic parameters*

In recent years an increase in the use of non-isothermal TG data to calculate rate-dependent parameters of solid-state decompositions has occurred, and several equations [19–26] have been employed. Many authors [19–23] have discussed the advantages of non-isothermal methods in comparison with isothermal ones.

The rate of a decomposition process can be described as the product of two separate functions of temperature and conversion rate [20]:

$$\frac{d\alpha}{dt} = k(T)f(\alpha) \tag{1}$$

where α is the fraction decomposed at time t, $k(T)$ is the temperature dependent function and $f(\alpha)$ is the conversion function dependent on the mechanism of decomposition. It has been established that the temperature dependent function $k(T)$ is of the Arrhenius type and can be considered as the rate constant k.

$$k = Ae^{-E^*/RT} \tag{2}$$

where R is the gas constant in ($J\,mol^{-1}\,K^{-1}$). Substituting equation (2) into equation (1), we get,

$$\frac{d\alpha}{dT} = \left(\frac{A}{\varphi e^{-E^*/RT}}\right) f(\alpha)$$

where ϕ is the linear heating rate dT/dt. On integration and approximation, this equation can be obtained in the following form

$$\ln g(\alpha) = -\frac{E^*}{RT} + \ln\left[\frac{AR}{\varphi E^*}\right]$$

where $g(\alpha)$ is a function of α, dependent on the reaction mechanism. Several techniques have been used for evaluation of the temperature integral. Most commonly used methods for this purpose are the differential method of Freeman and Carroll [19]; the integral method of Coats and Redfern [21] and the approximation method of Horowitz and Metzger [24].

The kinetic and thermodynamic parameters obtained for the metal caproates are summarized in table 5. Stability ranges, peak temperatures and values of kinetic parameters are shown in table 5. The data adjustments to Horowitz-Metzger (HM) and Coats-Redfern methods are graphically summarized in figure 5. Both methods give similar values for the parameters and exhibit the same trends for the metal cations.

From TG analysis, the most important and reliable kinetic parameter is the activation energy, which can be related to the thermal stability of the compounds and, in some cases, with some IR data. The copper compound has the highest value of E_a, suggesting a stronger metal-to-ligand interaction. Since Cu(II) has a [Ar] $3d^9$ configuration, the ligands may have a higher stabilization, in comparison with Zn(II), Cd(II), Pb(II) and Al(III). The strength of metal–ligand interactions will also be affected by the effective nuclear charge. The Cu(II) complex is the only one to exhibit a positive ΔS for the thermal degradation. This fact is probably related with the fact that this compound exhibits the higher ΔH value. In this process a solid (the compound) produces a new solid and a gaseous product. Hence, the overall ΔS value can be positive, as a consequence of the entropy changes in the gaseous and solid products (formation of a new crystalline lattice).

Table 5. Kinetic parameters to the studied caproates, from Coats-Redfern (CR) and Horowitz-Metzger (HM).

	Horowitz-Metzer						Coats-Redfen						
Complex	E (kJ mol^{-1})	Z (s^{-1})	ΔS (J mol^{-1} K^{-1})	ΔH (kJ mol^{-1})	ΔG (kJ mol^{-1})	R	E (kJ mol^{-1})	Z (s^{-1})	ΔS (J mol^{-1} K^{-1})	ΔH (kJ mol^{-1})	ΔG (kJ mol^{-1})	r	n
A	249.1	3.21E+21	161.7	244.6	155.4	0.9908	226.3	1.28E+19	115.8	221.8	157.9	0.9756	2.23
B	98.4	6.42E+05	−139.7	93.3	179.0	0.9845	81.8	1.43E+04	−171.4	76.7	181.8	0.9842	2.26
C	138.6	2.83E+09	−69.9	133.5	176.1	0.9775	126.3	1.30E+08	−95.5	121.3	179.5	0.9887	2.37
D	111.8	5.48E+06	−122.1	106.6	183.3	0.9823	100.8	3.85E+05	−144.2	95.6	186.2	0.9945	2.58
E	108.3	1.76E+08	−91.9	103.9	152.6	0.9748	102.5	2.91E+07	−106.8	98.1	154.7	0.9953	1.73

A, B, C, D and E are the Cu(II), Zn(II), Cd(II), Pb(II) and Al(III) caproates, respectively.

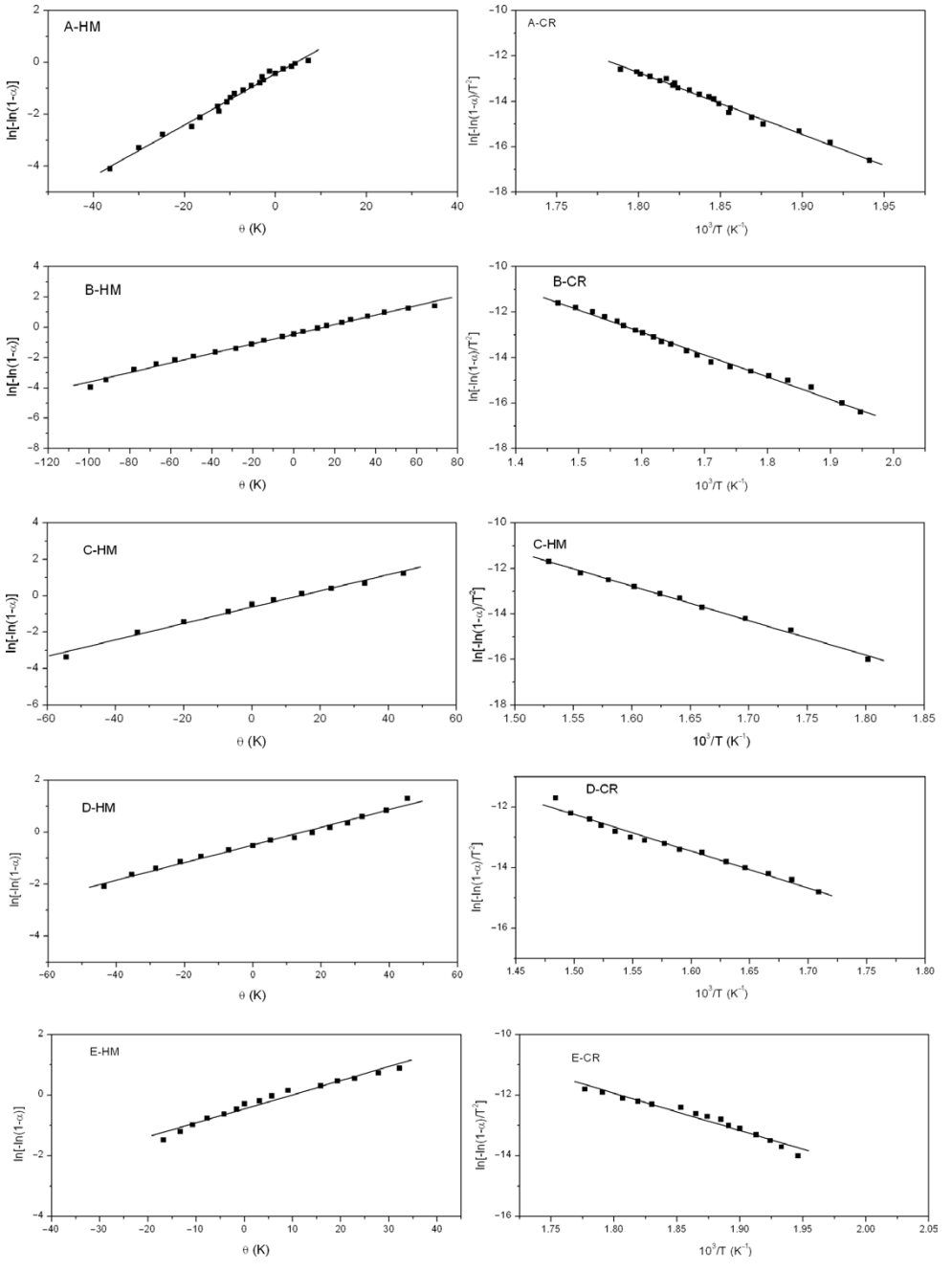

Figure 5. Horowitz-Metzger (HM) and Coats-Redfern (CR) plots for: (A) $Cu(cap)_2 \cdot 4H_2O$, (B) $Zn(cap)_2$, (C) $Cd(cap)_2 \cdot 4H_2O$, (D) $Pb(cap)_2$ and (E) $Al(cap)_3 \cdot 4H_2O$.

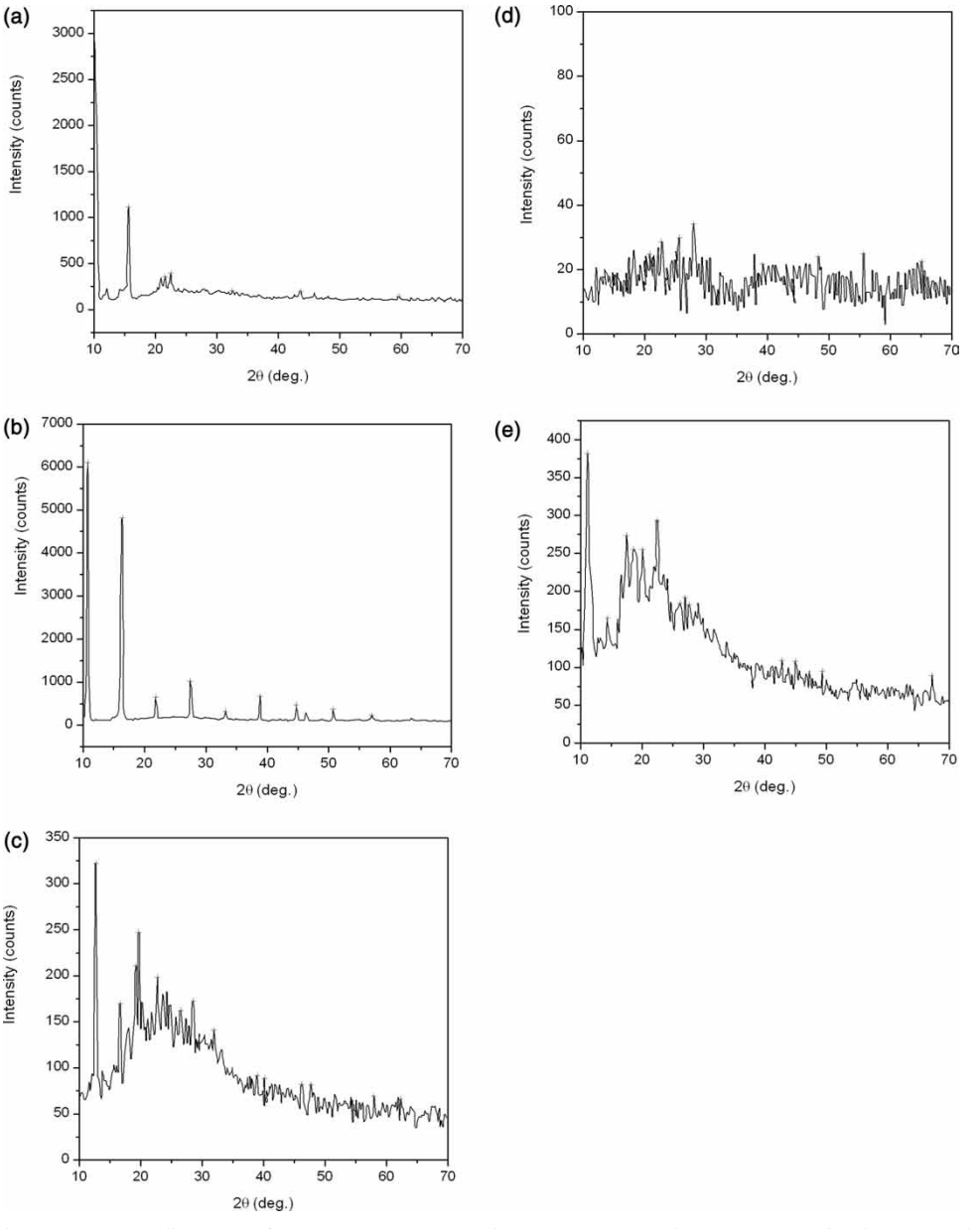

Figure 6. XRD diagrams of: (a) $Cu(cap)_2 \cdot 4H_2O$, (b) $Zn(cap)_2$, (c) $Cd(cap)_2 \cdot 4H_2O$, (d) $Pb(cap)_2$ and (e) $Al(cap)_3 \cdot 4H_2O$.

The higher E_a value for Cd(II) caproate in comparison to Zn(II), suggests that a larger cation stabilizes (provides a most stable crystalline lattice) a complex with two ligand molecules.

The ΔS values were negative (except $Cu(cap)_2 \cdot 4H_2O$) indicating a more ordered activated state through chemisorption of oxgen and other decomposition products [27]. The order of activation energy is $A > C > D \approx E > B$.

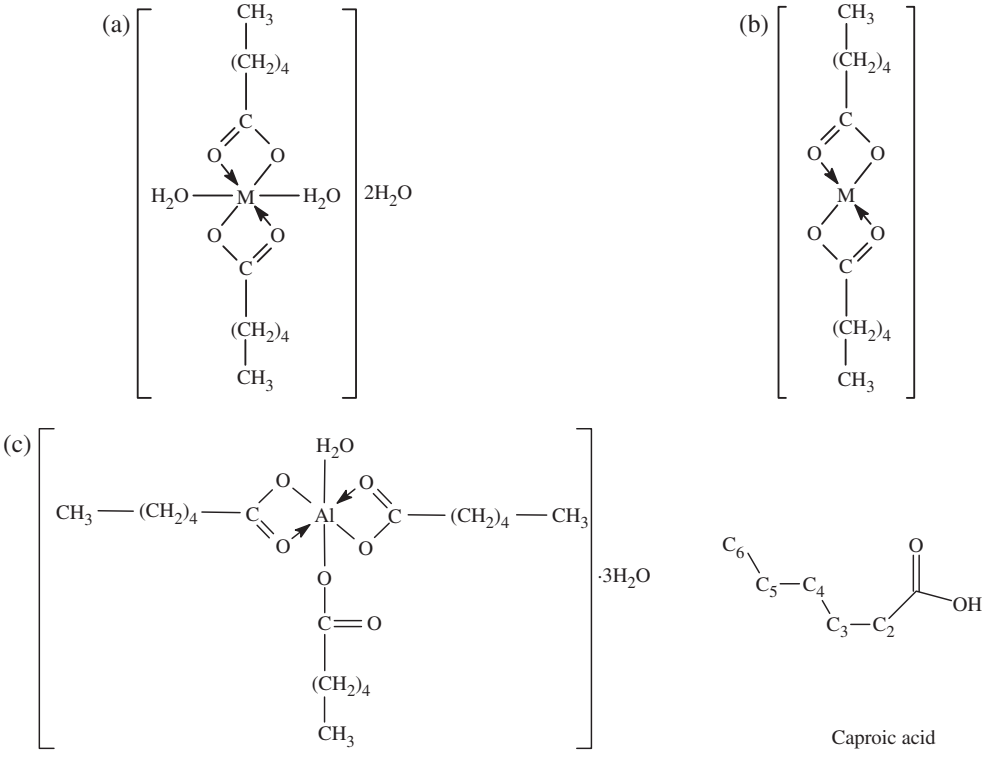

Figure 7. (a) The proposed structure for $Cu(cap)_2 \cdot 4H_2O$ and $Cd(cap)_2 \cdot 4H_2O$. (b) The proposed structure for $Zn(cap)_2$ and $Pb(cap)_2$. (c) The proposed structure for $Al(cap)_3 \cdot 4H_2O$.

3.6. *X-ray powder diffraction*

X-ray powder diffraction study of the compounds was carried out in order to examine the lattice dynamics. By comparison of the obtained X-ray powder diffraction patterns shown in figure 6, it is possible to verify that all compounds except lead) exhibit a diffraction peak in the range 11–13°. Furthermore, the copper, zinc and cadmium compounds exhibit another intense diffraction peak around 17°, suggesting that the compounds are isomorphs, with the zinc and lead compounds exhibiting the highest and lowest crystallinity, respectively. Although a complete indexation of the diffraction peaks was not performed, by comparison to the reported data for $Hg(N_2H_4CS)_4Zn(SCN)_4$ [28], the diffraction peaks could be tentatively attributed to the 200 and 310 diffraction peaks.

On the basis of above physiochemical data with consideration of ring strain, a distorted octahedral geometry (figure 7a) is proposed for the Cu-caproate complex. Zinc(II) and Pb(II) caproate complexes are tetrahedral (figure 7b) and an octahedral geometry (figure 7a and c) is proposed for Al(III) and Cd(II) complexes.

References

[1] S. Budavari (ed) *The Merck Index Text Book*, 12th Edn, p. 286, Rahway, NJ (1998).
[2] F. Beilstein. *Handbuch der Organischem Chemie*, Bd. IX, Springer Verlag, Berlin (1926).

[3] A. Zell, H. Einspahr, C.E. Bugg. *Biochem.*, **24**, 533 (1985).
[4] V.L. Pecoraro, M.J. Baldwin. A. Gelasco. *Chem. Rev.*, **94**, 807 (1994).
[5] R.C. Mehrotra, R. Bohra. *Metal Carboxylates*, Academic Press, London (1983).
[6] E.V. Brusau, J.C. Pedregosa, G.E. Narda, E.P. Ayala, E.A. Oliveira. *J. Arg. Chem. Soc.*, **92**(1/3), 43 (2004).
[7] T.N. Gushchina, G.A. Kotenko. *Koord. Khim.*, **12**(3), 325 (1986).
[8] W. Brzyska, B. Paszkowska. *J. Thermal Anal.*, **51**, 561 (1998).
[9] A. Doyle, J. Felcman, M. Gambardella, C.N. Verani, M.L.B. Tristao. *Polyhedron*, **19**(26/27), 2621 (2000).
[10] R. Pietsch. *Anal. Chim. Acta*, **53**(2), 287 (1971).
[11] L.L. Kolomiets, O.V. Lysenko, I.V. Pyatnitskii. *Z. Anal. Khim.*, **43**(10), 1773 (1988).
[12] I.V. Pyatnitskii, L.L. Kolomeits, O.V. Lysenko, M.G. Sobko. *Z. Anal. Khim.*, **45**(1), 56 (1990).
[13] S. Kopacz, J. Szantula, T. Pardela. *Z. Prikladoni Khim.*, **62**(11), 2535 (1989).
[14] G.B. Deacon, R.J. Phillips. *Coord. Chem. Rev.*, **33**, 227 (1980).
[15] N.W. Alcock, J. Culver, S.M. Roe. *J. Chem. Soc. Dalton Trans.*, 1447 (1992).
[16] K. Nakamoto. *Infrared and Raman Spectra of Inorganic and Coordination Compounds*, Wiley, New York (1997).
[17] B.R. Srinivasan, S.C. Sawant. *Thermochim. Acta*, **402**, 45 (2003).
[18] R. Murugavel, V.V. Karambelkar, G. Anantharaman, M.G. Walawalkar. *Inorg. Chem.*, **39**, 1381 (2000).
[19] E.S. Freeman, B. Carroll. *J. Phys. Chem.*, **62**, 394 (1958).
[20] J. Sestak, V. Satava, W.W. Wendlandt. *Thermochim. Acta*, **7**, 333 (1973).
[21] A.W. Coats, J.P. Redfern. *Nature*, **201**, 68 (1964).
[22] T. Ozawa. *Bull. Chem. Sot. Jpn.*, **38**, 1881 (1965).
[23] W.W. Wendlandt. *Thermal Methods of Analysis*, Wiley, New York (1974).
[24] H.W. Horowitz, G. Metzger. *Anal. Chem.*, **35**, 1464 (1963).
[25] J.H. Flynn, L.A. Wall. *Polym. Lett.*, **4**, 323 (1966).
[26] P. Kofstad. *Nature*, **179**, 1362 (1957).
[27] P.M. Madusudanan, K.K.M. Yasuff, C.G.R. Nair. *J. Therm. Anal.*, **8**, 31 (1975).
[28] X. Wang, D. Xu, X. Cheng, J. Huang. *J. Crystal Growth*, **271**, 120 (2004).